Geophysical Research Letters

RESEARCH LETTER
10.1029/2023GL105194

A Machine Learning-Based Approach to Quantify ENSO Sources of Predictability

Ioana Colfescu[1,2], **Hannah Christensen**[2], **and David John Gagne**[3]

[1]National Centre for Atmospheric Science (NCAS), University of Leeds, Leeds, UK, [2]Department of Atmospheric, Oceanic and Planetary Physics, University of Oxford, Oxford, UK, [3]National Center for Atmospheric Research, Boulder, CO, USA

Key Points:

- A deep learning-based approach suggests near-surface 10 m wind to play a significant role in providing skills for long-term ENSO predictability
- The skill of the 10-m zonal wind is large from 12 months up to 23 months in advance (depending on the season)
- The signal is generated by coupled wind-SST interactions in the Indian Ocean and later propagates across the Pacific

Supporting Information:

Supporting Information may be found in the online version of this article.

Correspondence to:

I. Colfescu,
ioana.colfescu@ncas.ac.uk

Citation:

Colfescu, I., Christensen, H., & Gagne, D. J. (2024). A machine learning-based approach to quantify ENSO sources of predictability. *Geophysical Research Letters*, *51*, e2023GL105194. https://doi.org/10.1029/2023GL105194

Received 24 JULY 2023
Accepted 13 APR 2024

Author Contributions:

Conceptualization: Hannah Christensen
Data curation: Ioana Colfescu
Formal analysis: Ioana Colfescu
Funding acquisition: Hannah Christensen
Investigation: Ioana Colfescu, Hannah Christensen, David John Gagne
Methodology: Ioana Colfescu, Hannah Christensen
Project administration: Hannah Christensen, David John Gagne
Resources: Hannah Christensen
Software: Ioana Colfescu, David John Gagne
Supervision: Hannah Christensen, David John Gagne
Validation: Ioana Colfescu

Abstract A machine learning method is used to identify sources of long-term ENSO predictability in the ocean (sea surface temperature (SST) and heat content) and the atmosphere (near-surface zonal wind (U10)). Tropical SST represents the primary source of predictability skill. While U10 does not increase the skill when associated with SST, our analysis suggests U10 alone has apredictive skill comparable to that of SST between 11 and 21 months in advance, from late fall up to late spring. The long-lead signal originates from coupled wind-SST interactions across the Indian Ocean (IO) and propagates across the Pacific via an atmospheric bridge mechanism. A linear correlation analysis supports this mechanism, suggesting a precursor link between anomalies in SST in the western and wind in the eastern IO. Our results have important implications for ENSO predictions beyond 1 year ahead and identify the key role of U10 over the IO.

Plain Language Summary Many extreme events, such as floods or droughts, can be attributed to the El Niño Southern Oscillation, a mode of large-scale ocean-atmosphere coupled variability in the tropical Pacific Ocean occurring with a period of approximately 4 years. In this analysis, we use a machine learning methodology to disentangle the key atmospheric and oceanic ENSO components' relative contribution to its predictability, particularly the role of near-surface 10-m zonal wind. We quantify the potential for improved ENSO predictions for up to 2 years in advance and present a mechanistic understanding of the location of the sources of predictability. While equatorial sea surface temperature represents the primary source of ENSO predictability, the equatorial U10 plays a vital role from late spring to fall, from 1 to 2 years in advance. The enhanced predictability skill is shown to be linked to an SST anomaly originating in the Indian Ocean. The ML model used provides a new way to get new insights into the sources of predictability for ENSO and can be used as a simple but powerful tool to improve the underlying mechanistic understanding.

1. Introduction

The signature pattern of El Niño Southern Oscillation (ENSO) is a higher-than-normal sea surface temperature (SST) anomaly in the equatorial eastern Pacific, accompanied by a weakening of the trade winds and a flattening of the thermocline (Philander, 1990). ENSO occurs approximately every 4 years and results in various climate impacts worldwide (e.g., Timmermann et al., 2018).

While ENSO exhibits diverse and irregular characteristics in its temporal evolution and spatial pattern (Capotondi et al., 2015, 2020; Chen & Jin, 2022; Wang, 2018), the physical mechanisms invoked to explain its occurrence fall essentially within two categories (Wang, 2018). One view describes ENSO as a self-sustained oscillatory mode of variability of the coupled ocean-atmosphere system (Suarez & Schopf, 1988; Weisberg & Wang, 1997; Wyrtki, 1975).

A second view originates from Hasselman's (1976) seminal paper which shows atmospheric weather noise to play an essential role in modulating SST variability (Colfescu & Schneider, 2020; Penland & Sardeshmukh, 1995). Accordingly, ENSO is interpreted as a damped mode of variability forced by stochastic atmospheric weather noise (Fedorov & Philander, 2000; Kessler & Kleeman, 2000; Moore & Kleeman, 1997; Roulston & Neelin, 2000). As a result of such stochastic patterns and the ENSO intrinsically irregular and partially nondeterministic nature, predicting ENSO events 6–12 months ahead represents a challenge for statistical and dynamical models.

Current dynamical forecast models can provide accurate predictions of ENSO events at lead times of about a year (Jin et al., 2008; Tippett et al., 2019; Zhang et al., 2021). In particular, while ENSO forecasts tend to remain

Visualization: Ioana Colfescu
Writing – original draft: Ioana Colfescu
Writing – review & editing: Ioana Colfescu

skillful (anomaly correlation coefficient above 0.5) during the mature phase of the cycle in boreal winter (Balmaseda et al., 1995), the skill decreases rapidly during the boreal spring when the amplitude of an ENSO event generally starts to grow (L'Hereux et al., 2017; Zhang et al., 2021). This feature, known as the spring predictability barrier (SPB), is characterized by a loss of autocorrelation in tropical SSTs, hindering ENSO predictability.

Improving ENSO predictions across the SPB and understanding the mechanisms behind it remain topics of extensive research (Wang, 2018). To address these challenges, recent studies have used artificial intelligence (AI) techniques (Dijkstra et al., 2019; Fang et al., 2022; Ham et al., 2021; Wang et al., 2023). Machine Learning (ML) approaches such as Artificial Neural Networks or Bayesian methods (Chen et al., 2021; Ham et al., 2019) have been employed to predict ENSO up to 2 years in advance, successfully outperforming dynamical models.

In this study, we build on the ML methodology used by Ham et al. (2019) to improve current understanding of the sources of ENSO forecast skill and their physical mechanism. Their studies used near-global SST and oceanic heat content (HC) as main predictors (Ham et al., 2019, 2021) and overlooked the potential role of wind anomalies. Yet, westerly bursts, for example, are believed to be crucial in influencing ENSO variability and timing (Fedorov et al., 2014; Hayashi & Watanabe, 2017; Tan et al., 2020).

The purpose of this study is threefold: (a) to investigate whether the long-term predictability skill can be improved, especially across the SPB, by using near-surface wind, U10, as a predictor; (b) to assess the interplay between atmospheric and oceanic predictors and isolate key geographical regions; and (c) to provide insights into the underpinning physical mechanism. Compared to Ham et al. (2019), the work provides a new understanding by examining separately the role of individual predictors, including new ones, by identifying the contribution of different geographical regions, and by providing insights into the physical mechanism in conjunction with a lead-lag correlation/regression analysis.

2. Data, Methods and Experiments

The convolutional neural network (CNN) model used here is described in detail in Ham et al. (2019, 2021). The input fields consist of a combination of 3-month rolling mean de-trended anomalies of SST, oceanic heat content (HC, defined as the vertically averaged temperature in the upper 300 m), and 10-m zonal wind (U10). Anomalies are computed relative to a climatology computed separately for each of the training, validation, and test periods. All input fields are regridded to a $5° \times 5°$ lat lon grid to reduce computational costs and to allow a direct comparison to Ham et al. (2019). We do not find significant differences in the ENSO predictive skill when using higher-resolution ($1° \times 1°$) input fields.

To train the CCN we used the first historical (1861–2001) ensemble member for 17 Coupled Model Intercomparison Project phase 5 (CMIP5, Taylor et al., 2012) models (see Table S1 in Supporting Information S1). As a validation data set, we used six ensemble members from the CMIP5 models (different from the ones used in the training period) for 1983–2014. The predictions (test runs) are performed for 1980–2014 using SST and HC from the Global Ocean Data Assimilation System (GODAS) reanalysis (Behringer et al., 1998) and U10 from the 20th Century Reanalysis v2c (Compo et al., 2011).

The main tests use input fields (SST, HC, U10, and various combinations of them) over the near-global ocean-only domain (0°–360°E, 55°S–60°N; D0 hereafter) and evaluate the predictability skill compared to that found using only SST and HC as input (as in Ham et al. (2021)). In addition, we also run several sensitivity tests with input variables prescribed over ocean-only sub-regional domains (see Table S1 in Supporting Information S1) to identify the contributions of various regions to the overall predictability skills and possible non-linearities. D1 is designed to isolate the contribution of the tropical Indo-Pacific; D2 explores the role of the western tropical Pacific where, for example, westerly wind bursts occur; D3 captures the influence of the near-equatorial Indian Ocean (IO), particularly around the centers of action of the Indian Ocean Dipole (IOD).

The CNN output consists of an array of 1–23-lead months representing the Niño3.4 index (3-month running mean area-averaged SST anomalies over 5°S–5°N, 170°–120°W) up to 2 years ahead. The skill of the ENSO forecasts is evaluated using the annual mean and the three-month-moving-average (i.e., 12 3-month seasons) correlation skill of the Niño3.4 index as a function of the forecast lead month (between 1 and 23).

To support the CCN-based results, an observational regression/correlation analysis of SST, U10, and HC on the Niño3.4 index is performed for the period 1875–2008. Data were taken from HadISST (Rayner et al., 2003), 20th

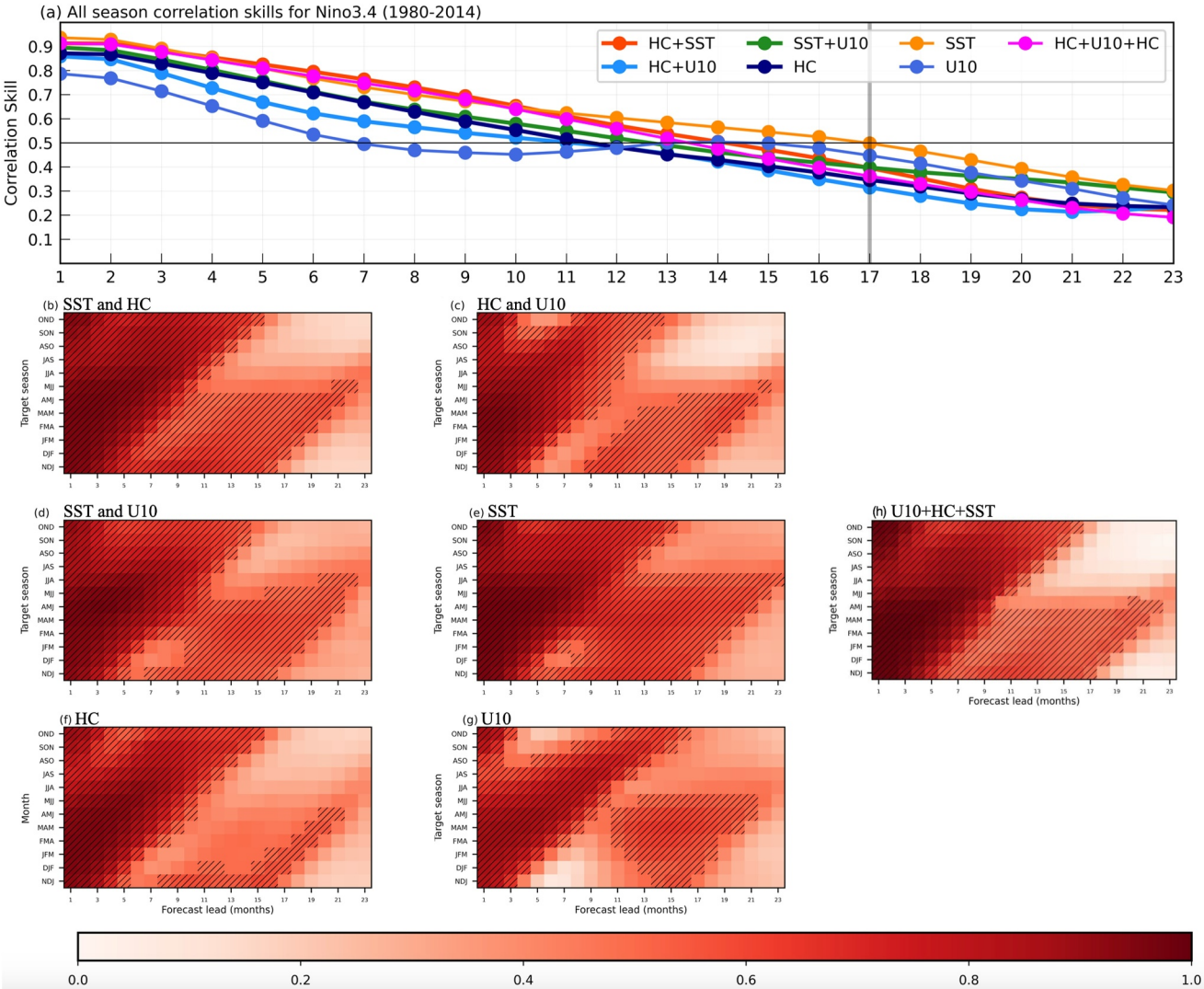

Figure 1. ENSO correlation skill in the CNN model for predictors over the near-global domain D0 (0°–360°E, 55°S–60°N). (a) The all-season correlation skill of the three-month-moving-average Niño3.4 index as a function of the forecast lead month. The different colors are associated with a different set of predictors: SST and HC (red), HC and U10 (light blue), SST and U10 (green), SST (orange), HC (dark blue), U10 (dark blue), U10 + HC + SST (pink). (b–h): The correlation skill of the Nino3.4 index for each of the 3-month seasons centered on each calendar month for the same experiments as in (a). Hatching in (b)–(h) highlights the forecasts with correlation skill exceeding 0.5.

Century Reanalysis v2c, and SODA v2.2.4 (Carton & Giese, 2008), respectively. The statistical significance of the anomalies is determined by the two-tailed Student's *t*-test.

3. Results

3.1. ENSO Forecast Skill With the CNN Model

The CNN-based annual mean correlation skill (based on monthly values) of the Niño3.4 index as a function of the forecast lead month is shown in Figure 1a, with the different time series representing the skill obtained using different sets of predictors. Figures 1b–1g display the corresponding skills for each of the 3-month running seasonal means. The forecast using SST and HC only as predictors represents the "reference forecast." Its all-seasons (annual) skill is above 0.5 for a lead time of up to 14 months (similarly to Ham et al. (2019)); there are, however, significant variations in the skill across the seasons. For example, Figure 1b shows that predictions targeting ENSO during the late boreal spring have successful skill (above 0.5) only for lead times up to 10 months. For ENSO during summer and fall, the lead time for successful predictions increases linearly, with relative

uniform values up to a sharp drop at leads around 11–15 months. Forecasts targeting ENSO during winter and early spring feature the largest skill (above 0.8) at short lead times (3–7 months), with a relatively large decrease at longer leads. Yet, the skill remains above 0.5 for lead times up to 16 months during early winter and reaches the maximum of 21 months for a target ENSO during MAM.

Examination of the role of different predictors and their combinations indicates that with SST alone the model can achieve an annual mean skill comparable to that using SST and HC combined (as in Ham et al. (2019)) for up to 11 months in advance, and to improve it for longer leads with useful predictions up to 17 months ahead. This indicates that the CNN model can learn the needed information only using SST as a predictor. This is a notable feature since, from a computational point of view, performing simulations with one predictor can significantly reduce resources and time. The seasonal distribution of the skill in the SST-only test closely resembles that of the reference forecast, with a minor degradation of the skill for fall and winter ENSO up to a lead of 11 months but a clear improvement for longer lead times, especially when targeting spring and winter ENSO (up to 0.2). Conversely, the skill decreases substantially using HC alone, especially for ENSO during winter and spring when predictions are unsuccessful if initialized more than 6–10 months in advance on average. The limit of useful predictions for late summer and fall ENSO is not significantly different from the reference case when using SST or HC (up 15 months ahead in all three tests). This again indicates that using SST alone as a predictor is enough in those seasons.

Turning to the predictability associated with U10, Figure 1a shows the skill to be substantially lower than that for any other predictor under 12 months in advance, and to noticeably decrease below 0.5 at month 7. However, the skill starts to increase at 10 months, reaching values around 0.5 between 13 and 15 months, and subsequently slowly decreases again. Remarkably, we find that U10 outperforms HC and SST + HC at leads longer than 14 months, with values close to those for SST alone. This suggests a potential source of long-lead ENSO predictability in U10. The seasonal distribution of the skill shows that the increase between 11 and 21 months is associated mainly with ENSO from winter to early summer. The use of U10 as a predictor, in addition to SST, appears to slightly deteriorate the predictions compared to those with SST alone, mostly at short leads (<12 months). We also find that the individual skills average up approximately linearly, which suggests a negligible influence of coupled processes among the chosen variables. Yet, the long-lead skill (>12 months in advance) remains above 0.5 for most of the fall to summer for SST alone. Conversely, U10 substantially improves the ENSO predictions based on HC alone at long leads, with valuable predictive skill at leads of 10–20 months in winter and spring, consistently with that of U10 alone.

Overall, the above analysis shows that the most considerable skill (>0.95) is found at short lead times (up to 4 months) and is essentially present throughout the year while also independent of the combination of chosen predictors, in agreement with other findings (Liu et al., 2022; Tang et al., 2018). At longer leads (>11 months), both SST and U10 in combination and separately provide considerable skill. The enhanced predictive skill at lead times between 11 and 21 months by using U10 warrants further investigations on its nature and origin (Section 3.2).

3.2. Origin of the Long-Lead Predictability Skill

While the CNN model runs analyzed in Section 3.1 used variables over D0, sensitivity tests were run to identify the region generating the long-lead predictive signal pointed out above, with the main results shown in Figure 2. This also provides insights into the underpinning mechanism (see also Section 3.3).

The all-season correlation skill for SST in the tropical Indo-Pacific region (D1) is almost identical to that in D0, with, for example, useful skill for up to nearly 16 months in advance as in Figure 1a. The only minor difference is the slight skill decrease at leads 6–11 months for D1. Physically, this indicates an overall negligible contribution of extra-tropical SST to the ENSO predictive skill, which results in more computationally efficient tests given the smaller domain of the predictor. The seasonal distribution of the skill confirms the similarity between the near-global and tropical-only SST tests, with the slight degradation in D1 attributable to ENSO predictions for winter and spring. Keeping the influence of SSTs over the IO and western Pacific only (D2) further reduces the skill by a relatively contained amount in the all-season skill at 1–9 months leads, with a mostly uniform decrease in all seasons. At long leads, there is a minor loss of predictability in late spring. Despite this further decrease, D2 captures the main features of the long-lead skill in D0, further highlighting the critical role of the western Pacific for long-lead ENSO predictions.

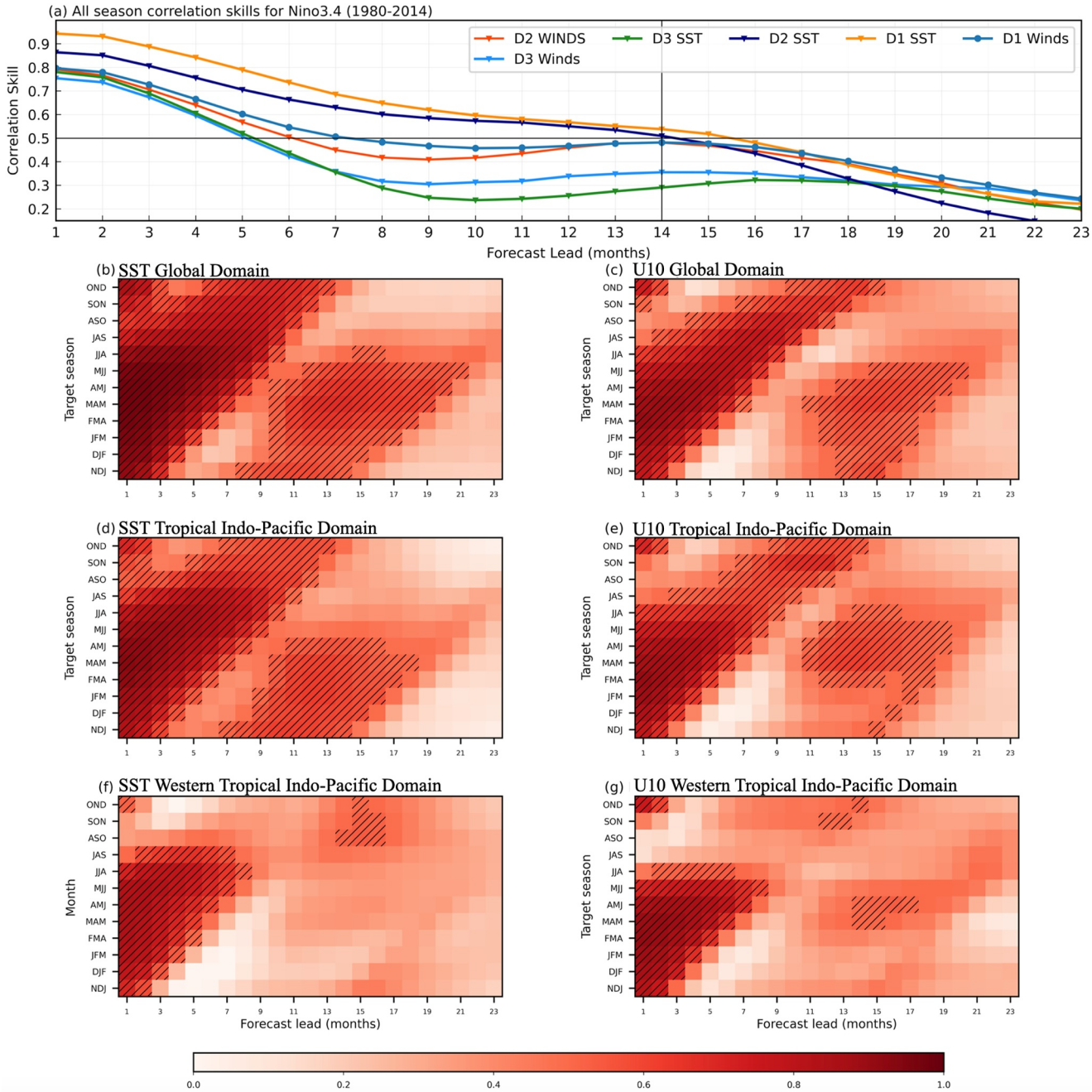

Figure 2. ENSO correlation skill in the CNN model for predictors over target areas (see Figure S1 in Supporting Information S1). (a) The all-season correlation skill of the three-month-moving-average Niño3.4 index as a function of the forecast lead month. The different colors are associated with a different set of predictors and areas namely, Global (D1 = 50°–290°E, 30°S–30°N); Tropical Indo Pacific (D2 = 65°–185°E, 50°S–40°N); Western Tropical Pacific (D3 = 50°–130°E, 50°S–20°N): SST D1 (orange), U10 D1 (steel blue), SST D2 (navy), U10 D2 (red), SST D3 (green), U10 D3 (light blue). (b–g): The correlation skill of the Nino3.4 index for each of the 3-month seasons centered on each calendar month for the same experiments as in (a). Hatching in (b)–(g) highlights the forecasts with correlation skill exceeding 0.5 and colorbar is the same as in Figure 1.

Sensitivity tests to the region of prescribed U10 display variations from the near-global simulation similar to those identified in the corresponding SST tests. The seasonal and all-season skills for D1 are essentially identical to those for D0, with no significant loss by restricting the domain to the tropics. The only exception is a slight degradation at 3–10 months lead time when targeting winter and early spring ENSO, possibly due to an influence of the extratropics. This behavior is more pronounced in D2, with a noticeable drop in the medium-term skill (5–

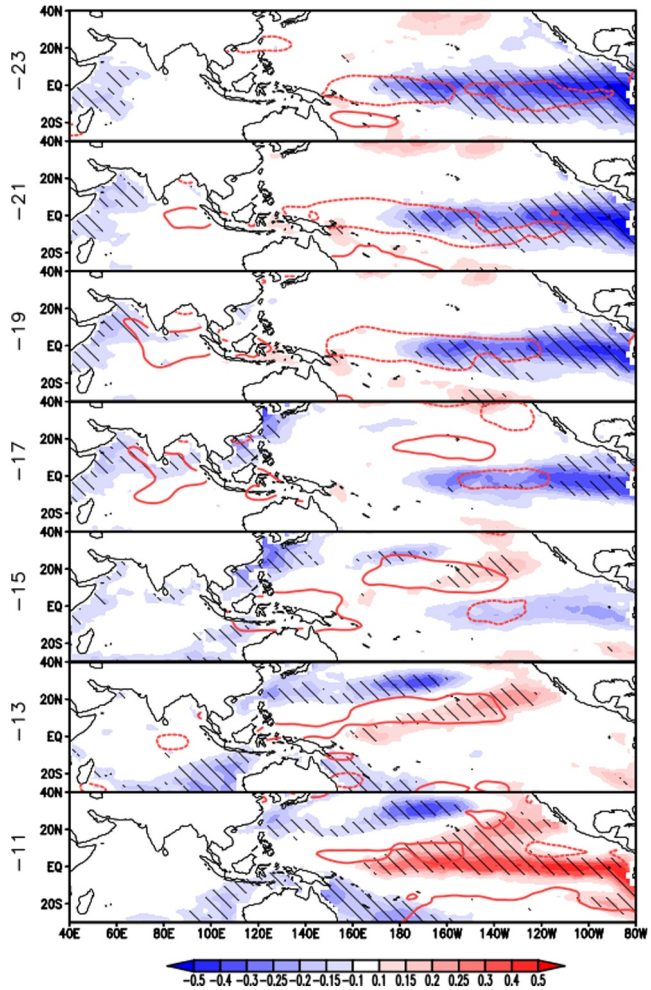

Figure 3. Regressions of monthly SST (shades) onto the March-April-May (MAM) Niño3.4 index. Hatching marks regions where the correlation between SST and the Niño3.4 index exceeds the 95% confidence level. The red contours indicate regions where the correlation between monthly U10 and the Niño3.4 index exceeds the 95% confidence level. Regressions/correlations are displayed at different lead times, namely from (top) $t = -23$ months to (bottom) $t = -11$ months ahead of the ENSO peak.

14 months ahead) during winter and spring. Yet, D2 still preserves significant skill in spring between 11 and 19 months ahead. We will return to this point later.

The weakest predictive skill—under 0.5 from lead 5 onwards—is associated with predictors in the IO (D3). Both the all-seasons and the seasonal correlation skills show few values above 0.5 beyond an 8-month lead time, with even a very poor skill in short-term predictions (up to 1 year in advance) for late summer and fall ENSO. One possible explanation for the overall poor ENSO predictive skill when using IO SST and U10 as predictors could be linked to the complex IOD pattern and its relationship to ENSO (Polonsky & Torbinsky, 2021), with a possible cancellation between the two action centers. Figures S2f and S2g in Supporting Information S1 show a complete lack of predictive skill in the fall season (starting with August–October), while the skill is resumed for more than 3 months in January–March. Conversely, Polonsky and Torbinsky (2021) found a significant (0.55) skill when the IOD precedes ENSO in the boreal autumn.

It is worth noticing that despite no predictive long-lead (10–15 months) skill with IO SST, the skill with U10 for March–May and April–June ENSO exceeds 0.5 (Figure 2g). To further investigate this issue and the possible cancellation between signals in the different IO sub-basins, two additional simulations were run by using SST and U10 over either the western or eastern IO (IODW and IODE, respectively; Figure S2 in Supporting Information S1). U10 in IODE displays the largest skill, even outperforming U10 in D3, particularly for the 10–17-month lead for spring ENSO. No such skill is present in SST. Noticeable are also the areas of negative skill and the out-of-phase relationship between the western and eastern sub-basins, possibly hinting at their reciprocal influence. Such a link is suggested by the similarity in the seasonal correlation skill patterns between SST in IODW and U10 in IODE, which leads to similar variations in the all-season skill with the lead month (despite the lower skill in IODW SST).

3.3. Mechanism in Observations

One may wonder whether the long-lead signal and, in particular, the potential of near-surface winds to be used as predictors for ENSO for 11–21 months in advance finds support in observations. This is important to ascertain whether the CNN-based ENSO predictions are rooted in physically plausible precursors. We thus carry out a seasonal regression/correlation analysis of U10, SST, and HC on the Niño3.4 index. For brevity, only anomalies regressed on ENSO during MAM (Figure 3) are shown, as one of the largest increases in the long-lead predictive skill in the CNN model occurs in this season (cfr. Figures 1 and 2).

About 23 months before the ENSO peak, a cold SST anomaly is present over the western equatorial IO, with significant values south of the equator (Figure S3a in Supporting Information S1). Weak and insignificant U10 and HC anomalies are found across the basin (Figure S3 in Supporting Information S1). Widespread cooling and anomalous easterlies exist over the central and eastern equatorial Pacific, surrounded by weaker sub-tropical warming (likely a residual of a previous La Niña). In the following months, the cold surface anomaly remains approximately constant in magnitude but extends northward across the Arabian Sea and then over the northern Bay of Bengal (the latter cooling likely associated with enhanced wind-induced evaporation), while no significant signal is seen in HC. This agrees with the CNN model's failure to identify much predictive skill when the HC is used as a predictor. Correspondingly, significant anomalous westerlies appear over the eastern equatorial IO from lead 21, which progressively strengthen and extend over the central and northern Indian Ocean until lead 17.

The regional wind anomalies (Figure S3b in Supporting Information S1) can be interpreted as the near-surface branch of a regional, zonal anomalous circulation cell induced by anomalous cooling and subsidence to the

west, with corresponding relatively warmer SST and ascent over the Eastern basin. As the westerlies over the IO increase, anomalous easterlies, stretching from the central basin, appear over the western equatorial Pacific. As shown in the wind patterns (Figure S3b in Supporting Information S1), this leads to low tropospheric convergence, thus contributing to the anomalous ascent and convection over Indonesia. In the ocean, the strengthening easterlies lead to significantly increased HC over the western Pacific. From lead 19, the easterly anomaly over the western equatorial Pacific starts migrating eastward, weakening and contracting in the zonal direction, while, simultaneously, the westerlies, previously confined to the IO, also move eastward and north-eastward across the Maritime continent and the western Pacific. The anomalous westerlies and cold SST anomalies in the IO weaken at lead 16, with muted signals by lead 12. In the Pacific, westerlies extend from Indonesia to the dateline at lead 14. Warm SST and HC anomalies increase and propagate north-westward and then spread equatorward by lead 12. This is followed by a rapid increase of westerly winds and SST over the eastern equatorial Pacific (via Bjerknes feedback), leading to the strong development of an ENSO event.

4. Discussion and Conclusions

This work sought to quantify the long-term predictability skill for ENSO using ML, to identify the relative contribution of different representative variables and geographical regions to the overall skill, and to provide insights into the underlying mechanism, particularly the role of near-surface zonal wind anomalies.

We find that skillful ENSO predictions for up to 17 months in advance in the all-season correlation skill can be achieved by using SST only as a predictor, with no need to include, for example, HC.

Compared to dynamical models, the predictability skill associated with SST is particularly marked for ENSO during late spring to early winter, with notable improvements across the SPB. The SST-only skill extends to long leads (>1.5 years) for ENSO from early winter to summer, when it approaches 23 months in advance. In contrast, predictions based on HC alone have useful all-season skills limited to only about 12 months. The most significant SST skill is associated with the tropical Indo-Pacific region, with either extratropical or Atlantic SST possibly contributing to the skill for winter and early spring predictions (>7 months ahead). SST represents the primary source of ENSO predictability. While U10 does not increase the skill when associated with SST, it can alone provide seasonal long-lead skill comparable to that of SST when targeting seasons from late fall to late spring and between 11 and 21 months in advance. In particular, a source of long-lead predictability skill for ENSO during spring and early summer (when dynamical models generally have the lowest skill) is associated with U10 in the IO. Using linear correlation/regression analysis, we suggest the skill to be mechanistically linked to preceding SST anomalies over the western IO and subsequent eastward propagation of the signal via wind anomalies.

A long-lead skillful prediction of ENSO has also been documented in other observationally based studies. For example, using a simple bilinear regression model with the IOD index and the equatorial Pacific warm water volume, Izumo et al. (2010) showed the IOD to be an efficient predictor of Niño3.4 up to 14 months before its peak. Using a composite analysis, Wieners et al. (2019) found prior independent information on ENSO in the western IO up to 15 months ahead, consistent with the results above. Interestingly, the ML predictive skill decreases markedly when using SST or winds limited to the IO or even including the western margin of the Maritime Continent, but is high when including the western Pacific. This would point to the critical role of atmospheric processes across Indonesia for ENSO predictions (the "atmospheric bridge") and the strong coupling between the Indian and Pacific oceans.

We do not find evidence for ocean dynamics in the IO (i.e., HC anomalies) to play a significant active role in the 11–21-month lead ENSO predictive skill as the oceanic signal is rather shallow and does not have longer memory than the SST. This suggests antecedent SST anomalies to be driven by atmospheric circulation changes (e.g., Wieners et al., 2019).

Also, in contrast to Ham et al. (2019), we show that the predictive skill can be obtained by using a single variable as a predictor (SST). This can be explained by recognizing that ENSO is a coupled atmospheric-ocean phenomenon; since the image recognition algorithm we are using has no intrinsic knowledge of the physics, it will "learn" similar information from either of the two coupled components—atmosphere or/and ocean. This hints at the enormous potential of using such methodologies in climate prediction, including the reduced computational costs compared to the coupled dynamical models, yet also highlights the need to combine such methods with a physical and mechanistic understanding.

This link between ENSO and antecedent (>1 year in advance) winds and SST anomalies in the IO has been recently suggested, with some studies pointing toward a link with the IOD (e.g., Chen et al., 2021; Izumo et al., 2010). While we do not investigate whether the remote IO wind anomaly originates/is linked to the previous ENSO (e.g., Zhang et al., 2021), the IOD, or their interplay, the results shown here allow us to isolate its contribution and usefulness for long-lead ENSO predictions. While previous studies suggest the need for improvements in the IO's observing system, we show that better model-based simulations of the zonal wind will benefit long-lead ENSO forecasts.

Although this study takes advantage of a large sample of data given by the CMIP5 experiments, the results will need to be confirmed by using, for example, the more recent CMIP6 models and the Single Model Initial-condition Large Ensembles (SMILEs, Deser et al., 2020). An interesting follow-up study would investigate the sensitivity of the results to the choice of the number of models, including accounting for inter-model dependencies (e.g., Boe' 2018), as well as to the domain and spatial resolution of the input data.

Data Availability Statement

All data sets used in this study are available on Zenodo (Colfescu, 2023).

Acknowledgments
IC was funded by the John Fell Oxford University Press Research Fund and HC by NERC (NE/P018238/1). The authors are grateful for the support from the UK JASMIN staff; the computational analysis has been performed on the UK JASMIN supercomputer. We thank Antje Weisheimer, Ed Schneider and Massimo Bollasina for their suggestions, and Jeong-Hwan Kim for helping with the ML model setup.

References

Balmaseda, M. A., Davey, M. K., & Anderson, D. L. T. (1995). Decadal and seasonal dependence of ENSO prediction skill. *Journal of Climate*, *8*(11), 2705–2715. https://doi.org/10.1175/1520-0442(1995)008<2705:DASDOE>2.0.CO;2

Behringer, D. W., Ji, M., & Leetmaa, A. (1998). An improved coupled model for ENSO prediction and implications for ocean initialization. Part I: The ocean data assimilation system. *Monthly Weather Review*, *126*(4), 1013–1021. https://doi.org/10.1175/1520-0493(1998)126

Boé, J. (2018). Interdependency in multimodel climate projections: Component replication and result similarity. *Geophysical Research Letters*, *45*(6), 2771–2779. https://doi.org/10.1002/2017GL076829

Capotondi, A., Wittenberg, A. T., Kug, J.-S., Takahashi, K., & McPhaden, M. J. (2020). ENSO diversity. In M. J. McPhaden, A. Santoso, & W. Cai (Eds.), *El Niño Southern Oscillation in a changing climate*. https://doi.org/10.1002/9781119548164.ch4

Capotondi, A., Wittenberg, A. T., Newman, M., Di Lorenzo, E., Yu, J. Y., Braconnot, P., et al. (2015). Understanding ENSO diversity. *Bulletin of the American Meteorological Society*, *96*(6), 921–938. https://doi.org/10.1175/BAMS-D-13-00117.1

Carton, J. A., & Giese, B. S. (2008). A reanalysis of ocean climate using simple ocean data assimilation (SODA). *Monthly Weather Review*, *136*(8), 2999–3017. https://doi.org/10.1175/2007MWR1978.1

Chen, H., & Jin, F. (2022). Dynamics of ENSO phase–Locking and its biases in climate models. *Geophysical Research Letters*, *49*(3), e2021GL097603. https://doi.org/10.1029/2021GL097603

Chen, N., Gilani, F., & Harlim, J. (2021). A Bayesian machine learning algorithm for predicting ENSO using short observational time series. *Geophysical Research Letters*, *48*(17), e2021GL093704. https://doi.org/10.1029/2021GL093704

Colfescu, I. (2023). A machine learning-based approach to quantify ENSO sources of predictability [Dataset]. https://doi.org/10.5281/zenodo.8385413

Colfescu, I., & Schneider, E. K. (2020). Decomposition of the Atlantic multidecadal variability in a historical climate simulation. *Journal of Climate*, *33*(10), 4229–4254. https://doi.org/10.1175/JCLI-D-18-0180.1

Compo, G. P., Whitaker, J. S., Sardeshmukh, P. D., Matsui, N., Allan, R. J., Yin, X., et al. (2011). The twentieth century reanalysis project. *Quarterly Journal of the Royal Meteorological Society*, *137*(654), 1–28. https://doi.org/10.1002/qj.776

Deser, C., Lehner, F., Rodgers, K. B., Ault, T., Delworth, T. L., DiNezio, P. N., et al. (2020). Insights from Earth system model initial-condition large ensembles and future prospects. *Nature Climate Change*, *10*(4), 277–286. https://doi.org/10.1038/s41558-020-0731-2

Dijkstra, H. A., Petersik, P., Hernández-García, E., & López, C. (2019). The application of machine learning techniques to improve El Niño prediction skill. *Frontiers in Physiology*, *7*, 153. https://doi.org/10.3389/fphy.2019.00153

Fang, W., Sha, Y., & Sheng, V. S. (2022). Survey on the application of artificial intelligence in ENSO forecasting. *Mathematics*, *10*(20), 3793. https://doi.org/10.3390/math10203793

Fedorov, A. V., Hu, S., Lengaigne, M., & Guilyardi, E. (2014). The impact of westerly wind bursts and ocean initial state on the development, and diversity of El Niño events. *Climate Dynamics*, *44*(5–6), 1381–1401. https://doi.org/10.1007/s00382-014-2126-4

Fedorov, A. V., & Philander, S. G. (2000). Is El Niño changing? *Science*, *288*(5473), 1997–2002. https://doi.org/10.1126/science.288.5473.1997

Ham, Y. G., Kim, J. H., Kim, E. S., & On, K. W. (2021). Unified deep learning model for El Niño/Southern Oscillation forecasts by incorporating seasonality in climate data. *Science Bulletin*, *66*(13), 1358–1366. https://doi.org/10.1016/j.scib.2021.03.009

Ham, Y. G., Kim, J. H., & Luo, J. J. (2019). Deep learning for multi-year ENSO forecasts. *Nature*, *573*(7775), 568–572. https://doi.org/10.1038/s41586-019-1559-7

Hasselmann, K. (1976). Stochastic climate models. Part I: Theory. *Tellus*, *28*(6), 473–485. https://doi.org/10.1111/j.2153-3490.1976.tb00696.x

Hayashi, M., & Watanabe, M. (2017). ENSO complexity induced by state dependence of westerly wind events. *Journal of Climate*, *30*(9), 3401–3420. https://doi.org/10.1175/JCLI-D-16-0406.1

Izumo, T., Vialard, J., Lengaigne, M., de Boyer Montegut, C., Behera, S. K., Luo, J. J., et al. (2010). Influence of the state of the Indian Ocean Dipole on the following year's El Niño. *Nature Geoscience*, *3*, 168–172. https://doi.org/10.1038/ngeo760

Jin, E. K., Kinter, J. L., Wang, B., Park, C. K., Kang, I. S., Kirtman, B. P., et al. (2008). Current status of ENSO prediction skill in coupled ocean-atmosphere models. *Climate Dynamics*, *31*(6), 647–664. https://doi.org/10.1007/s00382-008-0397-3

Kessler, W., & Kleeman, R. (2000). Rectification of the Madden-Julian oscillation into the ENSO cycle. *Journal of Climate*, *13*(20), 3560–3575. https://doi.org/10.1175/1520-0442(2000)013<3560:ROTMJO>2.0.CO;2

L'Heureux, M. L., Tippett, M. K., Kumar, A., Butler, A. H., Ciasto, L. M., Ding, Q., et al. (2017). Strong relations between ENSO and the Arctic Oscillation in the North American multimodel ensemble. *Geophysical Research Letters*, *44*(22), 11654–11662. https://doi.org/10.1002/2017GL074854

Liu, T., Song, X., Tang, Y., Shen, Z., & Tan, X. (2022). ENSO predictability over the past 137 years based on a CESM ensemble prediction system. *Journal of Climate*, *35*(2), 763–777. https://doi.org/10.1175/JCLI-D-21-0450.1

Moore, A. M., & Kleeman, R. (1997). The singular vectors of a coupled ocean-atmosphere model of ENSO. II: Sensitivity studies and dynamical interpretation. *Quarterly Journal of the Royal Meteorological Society*, *123*(540), 983–1006. https://doi.org/10.1002/qj.49712354010

Penland, C., & Sardeshmukh, P. D. (1995). The optimal growth of tropical sea surface temperature anomalies. *Journal of Climate*, *8*, 1999–2024. https://doi.org/10.1175/1520-0442(1995)008

Philander, S. G. (1990). *El Nino, La Nina, and the southern oscillation*. Academic Press.

Polonsky, A., & Torbinsky, A. (2021). The IOD–ENSO interaction: The role of the Indian Ocean current's system. *Atmosphere*, *12*, 1662. https://doi.org/10.3390/atmos12121662

Rayner, N. A., Parker, D. E., Horton, E. B., Folland, C. K., Alexander, L. V., Rowell, D. P., et al. (2003). Global analyses of sea surface temperature, sea ice, and night marine air temperature since the late nineteenth century. *Journal of Geophysical Research*, *108*(D14), 4407. https://doi.org/10.1029/2002jd002670

Roulston, M. S., & Neelin, J. D. (2000). The response of an ENSO model to climate noise, weather noise and intraseasonal forcing. *Geophysical Research Letters*, *27*(22), 3723–3726. https://doi.org/10.1029/2000GL011941

Suarez, M. J., & Schopf, P. S. (1988). A delayed action oscillator for ENSO. *Journal of the Atmospheric Sciences*, *45*(21), 3283–3287. https://doi.org/10.1175/1520-0469(1988)045<3283:ADAOFE>2.0.CO;2

Tan, X., Tang, Y., Lian, T., Zhang, S., Liu, T., & Chen, D. (2020). Effects of semistochastic westerly wind bursts on ENSO predictability. *Geophysical Research Letters*, *47*(14), e2019GL086828. https://doi.org/10.1029/2019GL086828

Tang, Y., Zhang, R.-H., Liu, T., Duan, W., Yang, D., Zheng, F., et al. (2018). Progress in ENSO prediction and predictability study. *National Science Review*, *5*(6), 826–839. https://doi.org/10.1093/nsr/nwy105

Taylor, K. E., Stouffer, R. J., & Meehl, G. A. (2012). An overview of CMIP5 and the experiment design. *Bulletin of the American Meteorological Society*, *93*(4), 485–498. https://doi.org/10.1175/BAMS-D-11-00094.1

Timmermann, A., An, S. I., Kug, J. S., Jin, F. F., Cai, W., Capotondi, A., et al. (2018). El Niño–Southern Oscillation complexity. *Nature*, *559*(7715), 535–545. https://doi.org/10.1038/s41586-018-0252-6

Tippett, M. K., Ranganathan, M., L'Heureux, M. L., Barnston, A. G., & DelSole, T. (2019). Assessing probabilistic predictions of ENSO phase and intensity from the North American Multimodel Ensemble. *Climate Dynamics*, *53*(12), 7497–7518. https://doi.org/10.1007/s00382-017-3721-y

Wang, C. (2018). A review of ENSO theories. *National Science Review*, *5*(6), 813–825. https://doi.org/10.1093/nsr/nwy104

Wang, G.-G., Cheng, H., Zhang, Y., & Yu, H. (2023). ENSO analysis and prediction using deep learning: A review. *Neurocomputing*, *520*, 216–229. https://doi.org/10.1016/j.neucom.2022.11.078

Weisberg, R. H., & Wang, C. (1997). A western Pacific oscillator paradigm for the El Niño-Southern Oscillation. *Geophysical Research Letters*, *24*(7), 779–782. https://doi.org/10.1029/97GL00689

Wieners, C. E., Dijkstra, H. A., & de Ruijter, W. P. M. (2019). The interaction between the western Indian Ocean and ENSO in CESM. *Climate Dynamics*, *52*(9–10), 5153–5172. https://doi.org/10.1007/s00382-018-4438-2

Wyrtki, K. (1975). El Niño—The dynamic response of the equatorial Pacific Oceanto atmospheric forcing. *Journal of Physical Oceanography*, *5*(4), 572–584. https://doi.org/10.1175/1520-0485(1975)005

Zhang, W., Jiang, F., Stuecker, M. F., Jin, F., & Timmermann, A. (2021). Spurious North tropical Atlantic precursors to El Niño. *Nature Communications*, *12*(1), 3096. https://doi.org/10.1038/s41467-021-23411-6